# UCLA

Title

Detrimental impact of aqueous mobile phases on 18F-labelled radiopharmaceutical analysis via radio-TLC

Permalink

https://escholarship.org/uc/item/7837f72g

Journal

Analytical Methods, 15(3)

ISSN

1759-9660

Authors

Laferriere-Holloway, Travis S
Rios, Alejandra
van Dam, R Michael

Publication Date

2023-01-19

DOI

10.1039/d2ay01206e

Peer reviewed

# Detrimental impact of aqueous mobile phases in 18F-labelled radiopharmaceutical analysis via radio-TLC

**Travis S. Laferriere-Holloway**[1,3], **Alejandra Rios**[2,3], **R. Michael van Dam**[1,2,3]

[1]Department of Molecular & Medical Pharmacology, David Geffen School of Medicine, University of California Los Angeles (UCLA), Los Angeles, CA, USA

[2]Physics and Biology in Medicine Interdepartmental Graduate Program, UCLA, Los Angeles, CA, USA

[3]Crump Institute for Molecular Imaging, UCLA, Los Angeles, CA, USA

## 1. INTRODUCTION

Positron-emission tomography (PET) is a non-invasive molecular imaging technique that harnesses radiopharmaceuticals to quantify biochemical processes *in vivo*. The radiopharmaceutical (or tracer) is a bioactive molecule labelled with a short-lived positron-emitting radionuclide. The most commonly used radionuclide is fluorine-18 due to its favorable physical and chemical properties.[1,2] Currently, most PET scans measure glucose metabolism with the radiopharmaceutical 2-[18F]fluoro-2-deoxy-D-glucose ([18F]FDG) to diagnose a myriad of diseases. However, additional types of scans may become more prevalent as several new PET tracers that are more specifically targeted to disease phenotypes have recently garnered clinical approval, including those targeting amyloid plaques (Neuraceq, Amyvid, Vizamyl), dysfunctional tau protein (Tauvid), prostate cancer (Axumin, Pylarify), and Parkinson's disease ([18F]FDOPA).[3] The list of new [18F]-labeled tracers under development also grows with the discovery of new biological targets and therapeutic strategies.[4]

The successful development and production of PET tracers rely on analytical techniques such as radio-high performance liquid chromatography (radio-HPLC) and radio-thin layer chromatography (radio-TLC) to assess radiochemical conversion (during radiosynthesis development) or radiochemical purity (during quality control testing of tracers produced for clinical use). A shortcoming of radio-HPLC, however, is the propensity for retention of free [18F]fluoride in the column (i.e., not reaching the detectors), which can lead to the

underestimation of this species in the output chromatogram.[5] In contrast, radio-TLC does not suffer from this issue as the entirety of the TLC plate is scanned.

When using typical silica TLC plates to separate $^{18}F$-labelled mixtures, $[^{18}F]$fluoride is usually sequestered near the origin through strong interaction with surface silanol groups, and the mobile phase moves the radiopharmaceutical away from the origin. The stationary phase, silica gel (polysilicic acid), is well known in the literature to possess the ability for acidic hydrogen bonding, basic hydrogen bonding, and dipolar interactions with analytes[6], and the mobile phase plays an important role in modulating these interactions. The reported mobile phases vary widely in literature, even for analysis of the same compound (Table 1), and we noted with interest that many studies use water as a polar mobile phase additive to enhance the migration of polar radiopharmaceutical compounds.

However, a drawback of using water is that it can alter the stationary phase itself through direct interactions of the water with surface silanol groups of the TLC plate. These modifications can disrupt the possible intermolecular interactions of the surface silanol groups, impeding plate-analyte interactions and adversely affecting chromatographic behavior.[7] In fact, under some conditions, the $[^{18}F]$fluoride-silica interaction can be disrupted, leading to the movement of free radionuclide away from the origin, which could lead to confusion and ambiguities in the analysis of $^{18}F$-radiopharmaceuticals if the TLC method is not carefully validated. We use systematic studies with different aqueous compositions to illustrate the potential detrimental impacts of using mobile phases with significant aqueous component on the radio-TLC analysis of tracers labeled with $[^{18}F]$fluoride and argue that the effects could also apply to tracers labelled with other radionuclides.

## 2.    EXPERIMENTAL

### 2.1    Materials and Methods

All reagents and solvents were obtained from commercial suppliers. Acetonitrile (MeCN; anhydrous, 99.8%), methanol (MeOH; anhydrous, 99.8%), water (H$_2$O; suitable for ion chromatography), 2,3-dimethyl-2-butanol (thexyl alcohol; anhydrous, 98%), N-methyl-2-pyrrolidone (NMP; anhydrous, 99.5%), 4,7,13,16,21,24-hexaoxa-1,10-diazabicyclo[8.8.8]hexacosane (K$_{222}$; 98%), and potassium carbonate (K$_2$CO$_3$; 99.995%), were purchased from Sigma-Aldrich (St. Louis, MO, USA). Tetrabutylammonium bicarbonate (TBAHCO$_3$; 75mM in ethanol), (2S)-O-(2$'$-tosyloxyethyl)-N-trityl-tyrosine-tert-butyl ester (TET; precursor for $[^{18}F]$FET, >95%), O-2-fluoroethyl-L-tyrosine (FET-HCl; reference standard, >95%), ethyl-5-methyl-8-nitro-6-oxo-5,6-dihydro-4H-benzo[f]imidazo[1,5-a][1,4]diazepine-3-carboxylate (nitromazenil; precursor for $[^{18}F]$Flumazenil, >97%), Flumazenil (FMZ; reference standard, >99%), (S)-2,3-dimethoxy-5-[3-[[(4-methylphenyl)-sulfonyl]oxy]-propyl]-N-[[1-(2-propenyl)-2-pyrrolidinyl]methyl]-benzamide ($[^{18}F]$Fallypride precursor, >90%), Fallypride (reference standard, >95%), were purchased from ABX Advanced Biochemical Compounds (Radeberg, Germany). Silica gel 60 F$_{254}$ sheets (aluminum backing, 5 cm × 20 cm) were purchased from Merck KGaA (Darmstadt, Germany). Glass

microscope slides (76.2 mm × 50.8 mm, 1 mm thick) were obtained from C&A Scientific (Manassas, VA, USA).

No-carrier-added [18F]fluoride was produced by the (p, n) reaction of [18O]H$_2$O (98% isotopic purity, Huayi Isotopes Co., Changshu, Jiangsu, China) in an RDS-111 cyclotron (Siemens, Knoxville, TN, USA) at 11 MeV, using a 1.2-mL silver target with havar foil.

## 2.2  Preparation of samples of [18F]fluoride and complexes

To illustrate the impact of aqueous mobile phases on the migration of [18F]fluoride, several samples were prepared.

[18F]fluoride samples were prepared by diluting [18F]fluoride/[18O]H$_2$O with ion chromatography-grade water to a concentration of 0.75–1.1 MBq/μL.

[18F]KF/K$_{222}$ samples were prepared by adding K$_2$CO$_3$ (0.5 mg, 3.6 μmol) and K$_{222}$ (5 mg, 13.3 μmol) to a volume of 0.5 mL of ion chromatography grade water spiked with [18F]fluoride, yielding a 0.75–1.1 MBq/μL solution with 7.2 mM K$_2$CO$_3$ and 26.2 mM K$_{222}$.

[18F]TBAF samples were prepared by adding TBAHCO$_3$ (75 mM; 1.2 μL, 0.7 μmol) to 99 uL of ion chromatography grade water spiked with [18F]fluoride to yield a 0.75–1.1 MBq/μL solution with 7.2 mM TBAHCO$_3$.

## 2.3  Preparation of samples of 18F-radiopharmaceuticals

To prepare mixed samples of radiotracers and [18F]fluoride, several radiopharmaceuticals were prepared using droplet radiochemistry methods on Teflon-coated silicon surface-tension trap chips as previously described[8]; except that optimal reaction conditions were altered to increase the amount of [18F]fluoride in the crude reaction mixture.

Mixtures of [18F]FET-intermediate/[18F]TBAF were prepared by depositing an 8 μL droplet of [18F]fluoride/[18O]H$_2$O (70–90 MBq [1.9–2.5 mCi]; mixed with 240 nmol of TBAHCO$_3$) and drying at 105 °C for 1 min. Then, the fluorination step was performed by adding a 10 μL droplet containing 80 nmol of FET precursor dissolved in thexyl alcohol:MeCN (1:1; v/v) to the dried [18F]fluoride residue and reacting at 90 °C for 5 min. The crude product was collected by dispensing 10 μL of MeCN to the reaction site and aspirating the volume. This process was repeated 6x for 60 μL of collected crude product.

Mixtures of [18F]FMZ/[18F]TBAF were prepared similarly, except that the fluorination step was performed by adding an 8 μL droplet containing 280 nmol of FMZ precursor dissolved in NMP to the dried [18F]fluoride residue and reacting at 200 °C for 0.5 min.

Mixtures of [18F]Fallypride/[18F]TBAF were prepared similarly, except that (i) the initial [18F]fluoride droplet contained 480 nmol of TBAHCO$_3$, and the fluorination step was performed by adding a 6 μL droplet containing 234 nmol of Fallypride precursor dissolved in thexyl alcohol:MeCN (1:1; v/v) to the dried [18F]fluoride residue and reacting at 110 °C for 1 min.

Stock solutions of non-radioactive reference standards were prepared at 20 mM concentration. 5 mg of Fallypride standard was added to 685 μL of MeOH. 5 mg of FMZ standard was added to 825 μL of MeOH. 5 mg of FET standard was added to 1100 μL of MeOH. MeOH was chosen due to the high solubility of these reference standards (as suggested by the manufacturer), and due to its relatively low boiling point that allowed rapid drying after spotting onto the TLC plate.

## 2.5 TLC spotting, developing, and readout

TLC plates were cut (6 cm long × 3 cm wide), then marked with a pencil at 1 cm (origin line) and 5 cm (development line) from the bottom edge. 1 μL of the relevant sample was applied to the plate via a micro-pipette. In cases where radiopharmaceutical solutions were separated, an adjacent lane on the plate was spotted with the corresponding reference standard. The sample spots were then dried under a gentle stream of nitrogen for 1 min. Spotting was repeated on multiple plates to compare the effect of different mobile phases containing MeCN with different amounts of $H_2O$ (all compositions expressed as v/v). After developing, plates were dried under a gentle stream of nitrogen for 3 min.

To better visualize the location of phase transfer catalysts ($TBAHCO_3$ and $K_2CO_3/K_{222}$), some plates were stained after developing by exposure for 1 min to a mixture of iodine crystals and silica gel in a sealed container.[9]

Plates were visualized via Cerenkov luminescence imaging (CLI) as previously described.[10,11] Briefly, the radio-TLC plate was positioned inside a light-tight chamber, then the plate was covered with a glass microscope slide. The Cerenkov light emission was detected by a cooled ($-10\ °C$) scientific camera (QSI 540, Quantum Scientific Imaging, Poplarville, MS, USA) equipped with a 50 mm F/1.2 lens (Nikkor, Nikon, Tokyo, Japan) for a 60 s exposure. In addition to previously described corrections, background subtraction was further performed by selecting a small region of the image (approximate size 20 pixels) not containing any radioactive species, computing the average pixel intensity, and subtracting this average from the entire image.

After CLI imaging, the glass microscope slide was removed, and a UV lamp installed inside the light-tight chamber was illuminated while acquiring another image of the plate (7 ms exposure time). This enabled visualization of chemical species on the plate (which appear as darker bands due to indicator present on the TLC plate), as well as capturing an image of pencil markings and iodine-stained bands on the plate.

## 2.6 Analysis of TLC plates

A MATLAB program (MathWorks, Natick, MA, USA) was written to generate TLC chromatograms and display TLC plate images. The user is first prompted to select the CLI image to be analyzed, followed by a corresponding darkfield image, and corrections are applied as previously described.[12] The program then asks the user to select a corresponding UV image, followed by selecting a flat field correction UV image (taken in advance with a blank TLC plate installed). The UV image is corrected in a similar fashion (i.e., dividing by the flat field correction image and applying 3×3 median filtering), and the user can further adjust brightness and contrast for viewing. The CLI image is then redisplayed, and the user

is asked to draw a line to define the width of the widest radioactivity band, which is used as the lane width. The UV image is then redisplayed, and the user is asked to draw a line from the bottom of the TLC plate to the solvent front. The program then generates an average line profile along the lane, taking the pixel intensities versus distance from the CLI image along the user-defined centerline and averaging with adjacent lines automatically generated at 1-pixel intervals along the entirety of the selected lane width. The program displays the final averaged line profile (chromatogram), the corrected CLI image, and the UV image.

The chromatogram was then exported and loaded in OriginPro (OrignLab, Northampton, MA, USA) to normalize the chromatograms to the highest intensity and plot groups of chromatograms. To compute the percentage of each species in a chromatogram, OriginPro was used to find the area under each band (peak) after fitting to a sum of Gaussian curves and then dividing the area corresponding to a particular band by the sum of areas for all bands.

## 3.  RESULTS AND DISCUSSION

Samples of $[^{18}F]$fluoride (with and without phase transfer catalysts) and various crude radiopharmaceuticals with different polarities were prepared and separated on silica TLC plates with different aqueous mobile phase compositions to illustrate the effect of water on the mobilization of different species and the potential pitfalls in analysis.

### 3.1  Effect of Aqueous Mobile Phases on Migration of $[^{18}F]$fluoride

Samples of $[^{18}F]$fluoride/$[^{18}O]H_2O$ were initially spotted on TLC plates and developed under mobile phases of increasing aqueous composition (Figure 1, Table 2). When the water content is low, $[^{18}F]$fluoride remains at the origin as expected. For   40% water, free $[^{18}F]$fluoride begins migrating away from the origin. Notably, and with great potential for ambiguity in the radio-TLC analysis of radiopharmaceuticals, two distinct bands of radioactivity are observed when using a mobile phase with   50% water. For   80% water composition, there is again only a single band observed, but it is located at the solvent front, near where the radiopharmaceutical species would be expected.

Recognizing that phase transfer catalysts are typically used in $^{18}F$-radiosyntheses, the behavior of complexed $[^{18}F]$fluoride was also investigated. Figure 2 and Table 3 show the effects of water on the movement of $[^{18}F]$TBAF (i.e., $[^{18}F]$fluoride in the presence of TBHACO$_3$). The overall trend is similar to free $[^{18}F]$fluoride, though there are increased signs of chromatographic fronting and band widening for some mobile phase compositions. This fronting may be explained because $[^{18}F]$fluoride and the phase transfer catalyst interact with one another yet have different migration behavior (Figure 2A). The migration of $[^{18}F]KF/K_{222}$ (i.e., $[^{18}F]$fluoride in the presence of $K_2CO_3$ and $K_{222}$) was also explored (Supplementary Figure S1 and Table S1) and shown to behave similarly to $[^{18}F]$TBAF.

### 3.3  Effect of Aqueous Mobile Phases on the Analysis of $[^{18}F]$Fallypride

Noting the effects that water composition had on the chromatographic behavior of $[^{18}F]$fluoride and its complexes, the effect of aqueous mobile phases on the chromatographic behavior of crude $[^{18}F]$Fallypride samples (containing unreacted $[^{18}F]$TBAF) was

investigated (Figure 3, Table 4). Interestingly, while [$^{18}$F]Fallypride is non-polar (cLogP = 3.3), using a mobile phase of 100% MeCN did not lead to migration away from the origin, and the [$^{18}$F]TBAF and [$^{18}$F]Fallypride bands could not be resolved. Increasing the water content to 20% caused the migration of [$^{18}$F]Fallypride toward the solvent front and allowed the bands to be resolved. However, for 40% water, there was decreased migration of [$^{18}$F]Fallypride (and further increased mobilization of [$^{18}$F]TBAF), and at 50% water, there was a significant overlap of the two species. Further addition of water ( 60%) led to a reversal in the order of the bands.

Under most TLC analyses performed, the radioactivity at the origin is generally assumed to be the free radionuclide, and the migrated species as the intermediate or product. Without careful assessment and validation of which bands correspond to which species, the overlapped or reversed results under the moderate or high proportion of water could introduce significant ambiguity and errors during analysis (Supplementary Figure S2).

### 3.4 Effect of Aqueous Mobile Phases on the Analysis of [$^{18}$F]FMZ

The effects of water composition were further investigated using samples of a more polar compound, [$^{18}$F]FMZ (cLogP = 1.0), containing [$^{18}$F]TBAF (Figure 4, Table 5). Though [$^{18}$F]FMZ is more polar than [$^{18}$F]Fallypride, the use of 100% MeCN led to the complete separation of [$^{18}$F]FMZ (near the solvent front) from [$^{18}$F]TBAF (at the origin). For 40% water, the [$^{18}$F]TBAF band begins to migrate away from the origin and split into two distinct radioactive bands, and for 60% water, mobilization of [$^{18}$F]FMZ begins to be adversely impacted. Significant overlap of the bands was observed using a 70% water mobile phase. Mobile phases with higher water content resulted in the migration of [$^{18}$F]TBAF to the solvent front, and [$^{18}$F]FMZ remained close to the origin. As mentioned previously, improper assumptions about the band locations could lead to significant misinterpretation of results (Supplementary Figure S3).

### 3.5 Effect of Aqueous Mobile Phases on the Analysis of [$^{18}$F]FET-intermediate

Next, the impact of aqueous mobile phases was assessed for crude mixtures of [$^{18}$F]FET-intermediate (cLogP = 3.9) containing [$^{18}$F]TBAF. Spotting of FET reference standard (cLogP = −0.9) in an adjacent lane allowed visualization of the impact of mobile phase composition on the analysis of 3 species (i.e., [$^{18}$F]TBAF, [$^{18}$F]FET-intermediate, and FET). With 100% MeCN, both [$^{18}$F]TBAF and FET remain at the origin, while the non-polar [$^{18}$F]FET-intermediate moves with the solvent front (Figure 5, Table 6). With 10% water, FET begins to move away from the origin, and with 40% water, [$^{18}$F]TBAF moves away from the origin, travelling close to FET. Interestingly, using 60% water impairs the mobility of the [$^{18}$F]FET-intermediate, which ends up closer to the origin with increasing water content, while [$^{18}$F]TBAF and FET remain overlapped at the solvent front. Supplementary Figure S4 shows the potential for the erroneous determination of radiochemical yield if the bands were improperly identified.

### 3.6 Discussion

These findings underscore water's complex role in chromatographic selectivity and highlight two major concerns about using water as a mobile phase additive for radiopharmaceutical

analysis on silica TLC plates. Firstly, the use of increasing amounts of water leads to a decreasing ability of the silica TLC plate to sequester [$^{18}$F]fluoride (and [$^{18}$F]fluoride complexes) at the origin, as well as the possibility that the [$^{18}$F]fluoride can form multiple bands when using a certain range of mobile phase compositions. Secondly, the water content can greatly affect the migration of the radiopharmaceutical species. Evidently, water plays a more important role in TLC plate selectivity than as a purely polar additive to affect analyte retention. These effects can lead to the overlap of bands at moderate water content and reversal of expected band positions at high water content, potentially leading to ambiguous or inaccurate determination of radiochemical compositions if TLC methods are not carefully validated.

A possible explanation for the first observation could be that water can convert silanol groups (Si-OH; isoelectric point ~2–3) to silanolate (Si-O$^-$) groups.[13] While silanol groups can act as weak ion exchangers and bind anionic [$^{18}$F]fluoride, silanolate groups do not possess this ion exchange capacity[14], potentially explaining the inability of the silica plates to sequester [$^{18}$F]fluoride at the origin when using mobile phases with moderate to high water percentages. This change in the TLC plate may also explain the reduced migration of polar radiopharmaceuticals for mobile phases with high water content, i.e., modification of the silanol groups could lead to greater analyte affinity.

Interestingly, the water content of the mobile phase also appears to strongly influence the migration of cationic radionuclides like [$^{68}$Ga]Ga$^{3+}$ on silica TLC plates. In a recent publication, researchers studied the effects of various mobile phases in the analysis of a $^{68}$Ga-labeled radiopharmaceutical[15], finding that with a 50% aqueous mobile phase, [$^{68}$Ga]Ga$^{3+}$ remains at the baseline, but for 100% aqueous mobile phases, [$^{68}$Ga]Ga$^{3+}$ migrated with the solvent front. This trend of mobilization for cationic species also appears to be true for other radionuclides like [$^{64}$Cu]Cu$^{2+}$, which have also been shown to move with the solvent front when using purely aqueous mobile phases[16], and it is possible that similar effects could be possible for other charged radionuclides (e.g., Sc-47, Zr-89, I-124, Lu-177, Ac-225). Further study is needed to better understand the chromatographic behavior of radiometals on silica TLC plates due to the complexity of these systems (e.g., different charge states of metal ions, possible coordination of metal ions with anions or solvents, and possible coordination with the surface functional groups).

## 4. Conclusions

Via systematic studies of different TLC mobile phase compositions and different $^{18}$F-labelled radiopharmaceuticals, we investigated the potential pitfalls of using water-containing mobile phases in TLC analysis of radiopharmaceuticals on silica TLC plates. Aqueous mobile phases with 30% water composition led to the migration of [$^{18}$F]fluoride (or complexes) away from the origin, with higher water content (~50%), leading to the splitting of the [$^{18}$F]fluoride band, and further increase of water content pushing [$^{18}$F]fluoride to the solvent front. Secondarily, it was found that moderate amounts of water could hinder the migration of the radiopharmaceutical and even cause overlap with the [$^{18}$F]fluoride band. While water is often used as a polar mobile phase additive in radiochemical analysis, the observations in this work highlight that water has, in fact, a more

complex role in chromatographic selectivity, and care is needed in radio-TLC interpretation when using mobile phases containing significant amounts of water. To avoid these complex effects, we are exploring facile methodologies for purely organic mobile phase optimization that can efficiently separate radiopharmaceuticals from radionuclides.

## Supplementary Material

Refer to Web version on PubMed Central for supplementary material.

## Acknowledgments

## REFERENCES

(1). Banister S; Roeda D; Dolle F; Kassiou M Fluorine-18 Chemistry for PET: A Concise Introduction. Curr. Radiopharm. 2010, 3 (2), 68–80. 10.2174/1874471011003020068.

(2). Jacobson O; Kiesewetter DO; Chen X Fluorine-18 Radiochemistry, Labeling Strategies and Synthetic Routes. Bioconjug. Chem. 2015, 26 (1), 1–18. 10.1021/bc500475e. [PubMed: 25473848]

(3). Drugs@FDA: FDA-Approved Drugs. https://www.accessdata.fda.gov/scripts/cder/daf/ (accessed 2022-07-18).

(4). Centre National de la Recherche Scientifique. 18F-Database of Imaging Radiolabelled Compounds (DIRAC). 18F-Database of Imaging Radiolabelled Compounds (DIRAC). http://www.iphc.cnrs.fr/dirac/ (accessed 2013-02-22).

(5). Ory D; Van den Brande J; de Groot T; Serdons K; Bex M; Declercq L; Cleeren F; Ooms M; Van Laere K; Verbruggen A; Bormans G Retention of [18F]Fluoride on Reversed Phase HPLC Columns. J. Pharm. Biomed. Anal. 2015, 111, 209–214. 10.1016/j.jpba.2015.04.009. [PubMed: 25898315]

(6). Snyder L Solvent Selectivity in Normal-Phase TLC. J. Planar Chromatogr. – Mod. TLC 2008, 21 (5), 315–323. 10.1556/JPC.21.2008.5.1.

(7). Johnson AR; Vitha MF Chromatographic Selectivity Triangles. J. Chromatogr. A 2011, 1218 (4), 556–586. 10.1016/j.chroma.2010.09.046. [PubMed: 21067756]

(8). Wang J; Chao PH; Dam RM van. Ultra-Compact, Automated Microdroplet Radiosynthesizer. Lab. Chip 2019, No. 19, 2415–2424. 10.1039/C9LC00438F. [PubMed: 31187109]

(9). Cardinale J; Martin R; Remde Y; Schäfer M; Hienzsch A; Hübner S; Zerges A-M; Marx H; Hesse R; Weber K; Smits R; Hoepping A; Müller M; Neels OC; Kopka K Procedures for the GMP-Compliant Production and Quality Control of [18F]PSMA-1007—A Next Generation Radiofluorinated Tracer for the Detection of Prostate Cancer. 2017. 10.20944/preprints201708.0057.v1.

(10). Wang J; Rios A; Lisova K; Slavik R; Chatziioannou AF; van Dam RM High-Throughput Radio-TLC Analysis. Nucl. Med. Biol. 2020, 82–83, 41–48. 10.1016/j.nucmedbio.2019.12.003.

(11). Sergeev M; Lazari M; Morgia F; Collins J; Javed MR; Sergeeva O; Jones J; Phelps ME; Lee JT; Keng PY; Dam RM van. Performing Radiosynthesis in Microvolumes to Maximize Molar Activity of Tracers for Positron Emission Tomography. Commun. Chem. 2018, 1 (1), 10. 10.1038/s42004-018-0009-z. [PubMed: 34291178]

(12). Dooraghi AA; Keng PY; Chen S; Javed MR; Kim C-J "CJ"; Chatziioannou AF.; van Dam RM. Optimization of Microfluidic PET Tracer Synthesis with Cerenkov Imaging. Analyst 2013, 138 (19), 5654–5664. 10.1039/C3AN01113E. [PubMed: 23928799]

(13). Wiegmann J The Chemistry of Silica. Solubility, Polymerization, Colloid and Surface Properties, and Biochemistry. Von RALPH K. ILER. New York/Chichester/Brisbane/Toronto: John Wiley

& Sons 1979.XXIV, 866 S., Lwd., £ 39.50. Acta Polym. 1980, 31 (6), 406–406. 10.1002/actp.1980.010310623.

(14). Dalstein L; Potapova E; Tyrode E The Elusive Silica/Water Interface: Isolated Silanols under Water as Revealed by Vibrational Sum Frequency Spectroscopy. Phys. Chem. Chem. Phys. 2017, 19 (16), 10343–10349. 10.1039/C7CP01507K. [PubMed: 28379259]

(15). Eppard E; Homann T; de la Fuente A; Essler M; Rösch F Optimization of Labeling PSMA $^{HBED}$ with Ethanol-Postprocessed $^{68}$Ga and Its Quality Control Systems. J. Nucl. Med. 2017, 58 (3), 432–437. 10.2967/jnumed.116.177634. [PubMed: 28082433]

(16). Jeong S; Park JY; Cha MG; Chang H; Kim Y; Kim H-M; Jun B-H; Lee DS; Lee Y-S; Jeong JM; Lee Y-S; Jeong DH Highly Robust and Optimized Conjugation of Antibodies to Nanoparticles Using Quantitatively Validated Protocols. Nanoscale 2017, 9 (7), 2548–2555. 10.1039/C6NR04683E. [PubMed: 28150822]

(17). Lazari M; Collins J; Shen B; Farhoud M; Yeh D; Maraglia B; Chin FT; Nathanson DA; Moore M; Dam RM van. Fully Automated Production of Diverse 18F-Labeled PET Tracers on the ELIXYS Multireactor Radiosynthesizer Without Hardware Modification. J. Nucl. Med. Technol. 2014, 42 (3), 203–210. 10.2967/jnmt.114.140392. [PubMed: 25033883]

(18). Lu S; Giamis AM; Pike VW Synthesis of [18F]Fallypride in a Micro-Reactor: Rapid Optimization and Multiple-Production in Small Doses for Micro-PET Studies. Curr. Radiopharm. 2009, 2 (1), 1–13.

(19). Inkster J. a. H.; Akurathi V.; Sromek AW.; Chen Y.; Neumeyer JL.; Packard AB. A Non-Anhydrous, Minimally Basic Protocol for the Simplification of Nucleophilic 18 F-Fluorination Chemistry. Sci. Rep. 2020, 10 (1), 1–9. 10.1038/s41598-020-61845-y. [PubMed: 31913322]

(20). Ismail R; Irribarren J; Javed MR; Machness A; van Dam M; Keng PY Cationic Imidazolium Polymer Monoliths for Efficient Solvent Exchange, Activation and Fluorination on a Continuous Flow System. RSC Adv. 2014, 4 (48), 25348–25356. 10.1039/c4ra04064c.

(21). Lisova K; Wang J; Hajagos TJ; Lu Y; Hsiao A; Elizarov A; van Dam RM Economical Droplet-Based Microfluidic Production of [18F]FET and [18F]Florbetaben Suitable for Human Use. Sci. Rep. 2021, 11 (1), 20636. 10.1038/s41598-021-99111-4. [PubMed: 34667246]

(22). Wessmann SH; Henriksen G; Wester H-J Cryptate Mediated Nucleophilic 18F-Fluorination without Azeotropic Drying. Nukl. Nucl. Med. 2012, 51 (1), 1–8. 10.3413/Nukmed-0425-11-08.

(23). Bogni A; Laera L; Cucchi C; Iwata R; Seregni E; Pascali C An Improved Automated One-Pot Synthesis of O-(2-[18F]Fluoroethyl)-L-Tyrosine ([18F]FET) Based on a Purification by Cartridges. Nucl. Med. Biol. 2019, 72–73, 11–19. 10.1016/j.nucmedbio.2019.05.006.

(24). Wang M-W; Yin D-Z; Zhang L; Zhou W; Wang Y-X Remote-Controlled Module-Assisted Synthesis of O-(2-[18F]Fluoroethyl)-L-Tyrosine as Tumor PET Tracer Using Two Different Radiochemical Routes. Nucl. Sci. Tech. 2006, 17 (3), 148–153. 10.1016/S1001-8042(06)60029-8.

(25). Wang H; Guo X; Jiang S; Tang G Automated Synthesis of [18F]Florbetaben as Alzheimer's Disease Imaging Agent Based on a Synthesis Module System. Appl. Radiat. Isot. 2013, 71 (1), 41–46. 10.1016/j.apradiso.2012.09.014. [PubMed: 23085550]

(26). Wang J; Holloway T; Lisova K; Dam RM van. Green and Efficient Synthesis of the Radiopharmaceutical [18F]FDOPA Using a Microdroplet Reactor. React. Chem. Eng. 2020, 5 (2), 320–329. 10.1039/C9RE00354A. [PubMed: 34164154]

(27). Wang YX; Zhang L; Tang GH; Yin DZ An Improved Enantioselective Synthesis of No-Carrier-Added (NCA) 6-[18F]FLUORO-L-DOPA. J. Label. Compd. Radiopharm. 2001, 44 (S1), S866–S867. 10.1002/jlcr.25804401304.

(28). Libert LC; Franci X; Plenevaux AR; Ooi T; Maruoka K; Luxen AJ; Lemaire CF Production at the Curie Level of No-Carrier-Added 6-18F-Fluoro-l-Dopa. J. Nucl. Med. 2013, 54 (7), 1154–1161. 10.2967/jnumed.112.112284. [PubMed: 23658219]

(29). Shen B; Ehrlichmann W; Uebele M; Machulla H-J; Reischl G Automated Synthesis of n.c.a. [18F]FDOPA via Nucleophilic Aromatic Substitution with [18F]Fluoride. Appl. Radiat. Isot. 2009, 67 (9), 1650–1653. 10.1016/j.apradiso.2009.03.003. [PubMed: 19433364]

(30). F L.; Jw H.; L Y.; L D.; L M.; J H.; T L. Plasma Radio–Metabolite Analysis of PET Tracers for Dynamic PET Imaging: TLC and Autoradiography. 2020. 10.21203/rs.3.rs-35592/v3.

(31). Stephenson NA; Holland JP; Kassenbrock A; Yokell DL; Livni E; Liang SH; Vasdev N Iodonium Ylide Mediated Radiofluorination of 18F-FPEB and Validation for Human Use. J. Nucl. Med. 2015, 56 (3), 489–492. 10.2967/jnumed.114.151332. [PubMed: 25655630]

(32). Nandy SK; Rajan MGR Fully Automated and Simplified Radiosynthesis of [18F]-3′-Deoxy-3′-Fluorothymidine Using Anhydro Precursor and Single Neutral Alumina Column Purification. J. Radioanal. Nucl. Chem. 2009, 283 (3), 741–748. 10.1007/s10967-009-0429-4.

(33). Lee SJ; Oh SJ; Chi DY; Kil HS; Kim EN; Ryu JS; Moon DH Simple and Highly Efficient Synthesis of 3′-Deoxy-3′-[18F]Fluorothymidine Using Nucleophilic Fluorination Catalyzed by Protic Solvent. Eur. J. Nucl. Med. Mol. Imaging 2007, 34 (9), 1406–1409. 10.1007/s00259-007-0391-8. [PubMed: 17384949]

(34). Vaulina D; Nasirzadeh M; Gomzina N Automated Radiosynthesis and Purification of [18F]Flumazenil with Solid Phase Extraction. Appl. Radiat. Isot. 2018, 135, 110–114. 10.1016/j.apradiso.2018.01.008. [PubMed: 29413823]

(35). Nasirzadeh M; Vaulina DD; Kuznetsova OF; Gomzina NA A Novel Approach to the Synthesis of [18F]Flumazenil, a Radioligand for PET Imaging of Central Benzodiazepine Receptors. Russ. Chem. Bull. 2016, 65 (3), 794–800. 10.1007/s11172-016-1376-1.

(36). Ryzhikov NN; Gomzina NA; Fedorova OS; Vasil'ev DA; Kostikov AP; Krasikova RN Preparation of [18F]Flumazenil, a Potential Radioligand for PET Imaging of Central Benzodiazepine Receptors, by Isotope Exchange. Radiochemistry 2004, 46 (3), 290–294. 10.1023/B:RACH.0000031692.63830.85.

(37). Akula MR; Collier TL; Blevins DW; Kabalka GW; Osborne D Sequential Preparation of [18F]FLT and [18F]FMISO Employing Advion NanoTek® Microfluidic Synthesis System. Adv. Mol. Imaging 2019, 9 (4), 53–59. 10.4236/ami.2019.94008.

(38). Collins J; Waldmann CM; Drake C; Slavik R; Ha NS; Sergeev M; Lazari M; Shen B; Chin FT; Moore M; Sadeghi S; Phelps ME; Murphy JM; Dam RM van. Production of Diverse PET Probes with Limited Resources: 24 ^{18}F-Labeled Compounds Prepared with a Single Radiosynthesizer. Proc. Natl. Acad. Sci. 2017, 114 (43), 11309–11314. 10.1073/pnas.1710466114. [PubMed: 29073049]

(39). Zarganes-Tzitzikas T; Clemente GS; Elsinga PH; Dömling A MCR Scaffolds Get Hotter with 18F-Labeling. Molecules 2019, 24 (7), 1327. 10.3390/molecules24071327. [PubMed: 30987302]

(40). Russelli L; Martinelli J; De Rose F; Reder S; Herz M; Schwaiger M; Weber W; Tei L; D'Alessandria C Room Temperature Al18F Labeling of 2-Aminomethylpiperidine-Based Chelators for PET Imaging. ChemMedChem 2020, 15 (3), 284–292. 10.1002/cmdc.201900652. [PubMed: 31830368]

(41). Yu H-M; Chan C-H; Yang C-H; Hsia H-T; Wang M-H Hexavalent Lactoside Labeled with [18F]AlF for PET Imaging of Asialoglycoprotein Receptor. Appl. Radiat. Isot. 2020, 162, 109199. 10.1016/j.apradiso.2020.109199. [PubMed: 32501233]

(42). Shih I-H; Duan X-D; Kong F-L; Williams MD; Yang K; Zhang Y-H; Yang DJ Automated Synthesis of 18F-Fluoropropoxytryptophan for Amino Acid Transporter System Imaging. BioMed Res. Int. 2014, 2014, e492545. 10.1155/2014/492545.

(43). Ungersboeck J; Richter S; Collier L; Mitterhauser M; Karanikas G; Lanzenberger R; Dudczak R; Wadsak W Radiolabeling of [18F]Altanserin — a Microfluidic Approach. Nucl. Med. Biol. 2012, 39 (7), 1087–1092. 10.1016/j.nucmedbio.2012.04.004. [PubMed: 22633218]

(44). Koivula T; Laine J; Lipponen T; Perhola O; Kämäräinen E-L; Bergström K; Solin O Assessment of Labelled Products with Different Radioanalytical Methods: Study on 18F-Fluorination Reaction of 4-[18F]Fluoro-N-[2-[1-(2-Methoxyphenyl)-1-Piperazinyl]Ethyl-N-2-Pyridinyl-Benzamide (p-[18F]MPPF). J. Radioanal. Nucl. Chem. 2010, 286 (3), 841–846. 10.1007/s10967-010-0802-3.
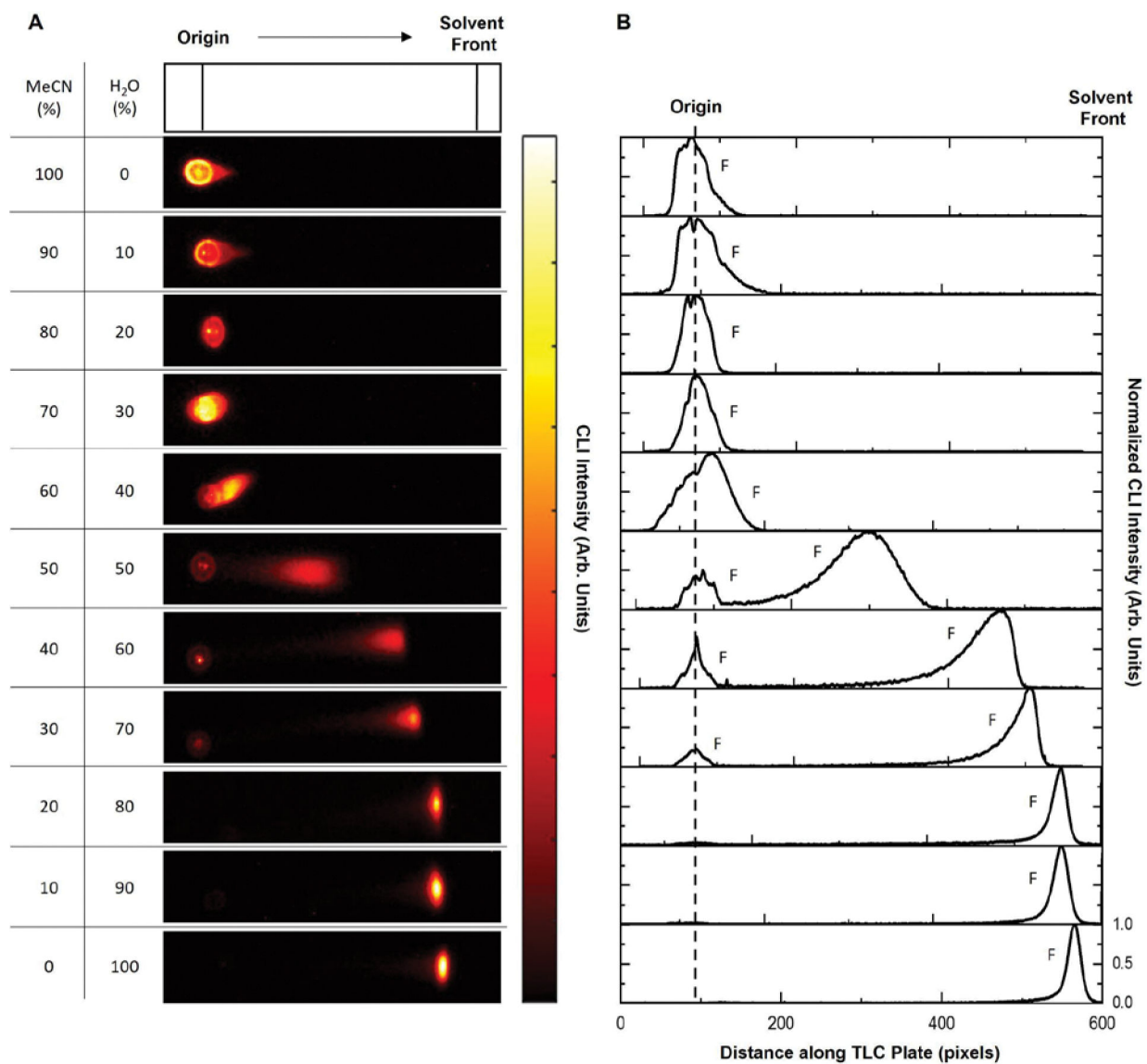
**Figure 1.**
Impact of water composition in aqueous mobile phases (MeCN:H$_2$O) on the migration of [$^{18}$F]fluoride. **(A)** CLI images of TLC plates. **(B)** TLC chromatograms generated from the CLI images. F denotes [$^{18}$F]fluoride.
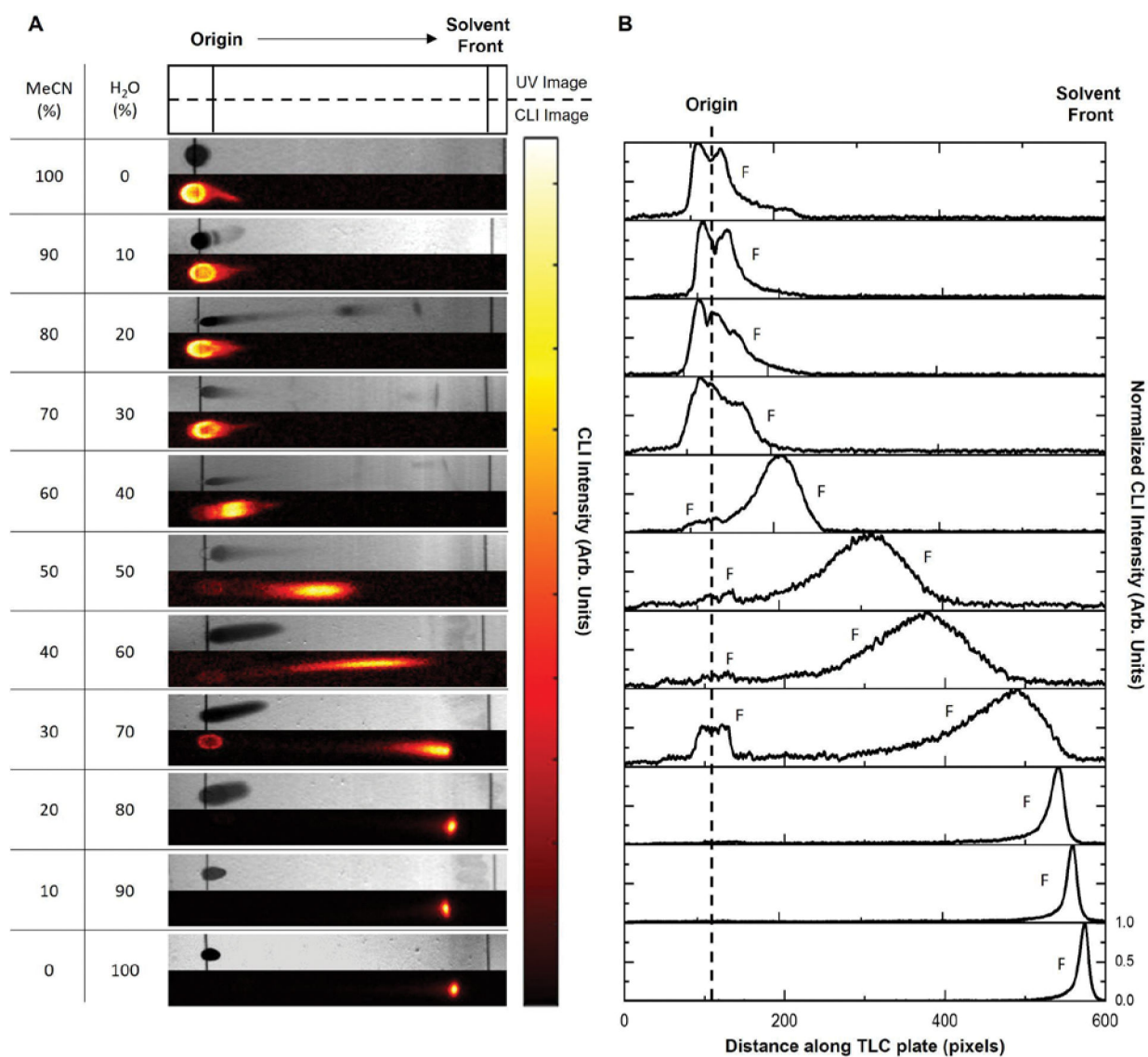
**Figure 2.**

The effect of aqueous mobile phases (MeCN:H$_2$O) on the migration of [$^{18}$F]TBAF. **(A)** For each mobile phase composition, two images are shown: a UV image of the TLC plate stained with I$_2$ to visualize TBAHCO$_3$ (top), and a CLI image of a TLC plate spotted with [$^{18}$F]TBAF (bottom). **(B)** Normalized TLC chromatograms generated from the CLI images. F denotes [$^{18}$F]TBAF. The Supplementary Information contains an additional figure showing the migration of samples of [$^{18}$F]KF/K$_{222}$.
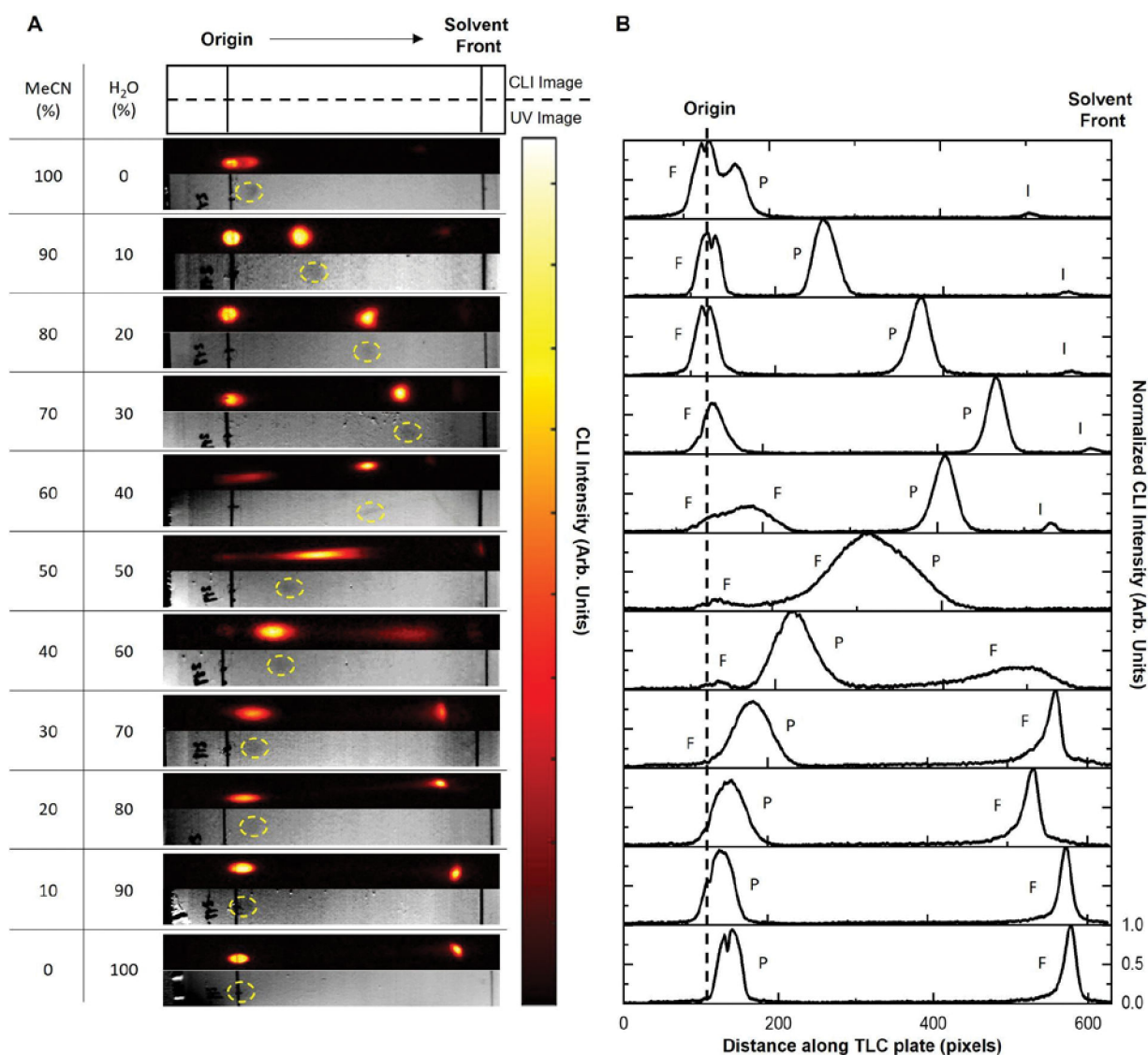
**Figure 3.**
Impact of water composition in aqueous mobile phases (MeCN:H$_2$O) on the migration of [$^{18}$F]Fallypride. **(A)** Images of TLC plates. For each mobile phase composition, a CLI image of the TLC plate spotted with crude [$^{18}$F]Fallpyride is shown (top), along with a UV image of an adjacent lane spotted with Fallypride standard (bottom). The Fallypride standard band is enclosed with a yellow dashed line for clarity. **(B)** Normalized TLC chromatograms generated from the CLI images. F denotes [$^{18}$F]TBAF, P denotes [$^{18}$F]Fallypride, and I denotes impurity.
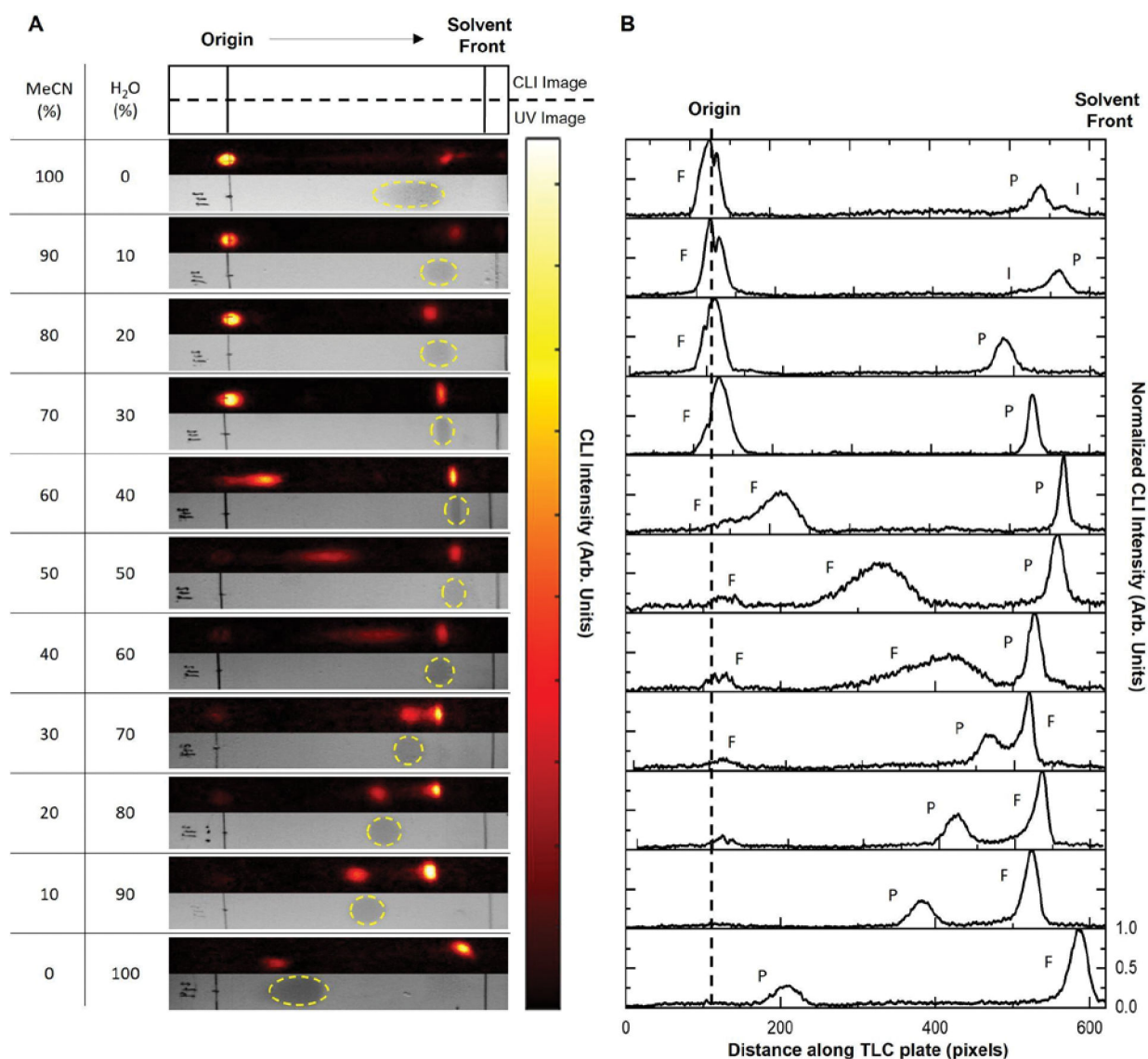
**Figure 4.**
Impact of water composition in aqueous mobile phases (MeCN:H$_2$O) on the migration of [$^{18}$F]FMZ. **(A)** Images of TLC plates. For each mobile phase composition, a CLI image of the TLC plate spotted with crude [$^{18}$F]FMZ is shown (top), along with a UV image of an adjacent lane spotted with FMZ reference standard (bottom). The FMZ standard band is enclosed with a yellow dashed line for clarity. **(B)** Normalized TLC chromatograms generated from the CLI images. F denotes [$^{18}$F]TBAF, P denotes [$^{18}$F]FMZ, and I denotes impurity.
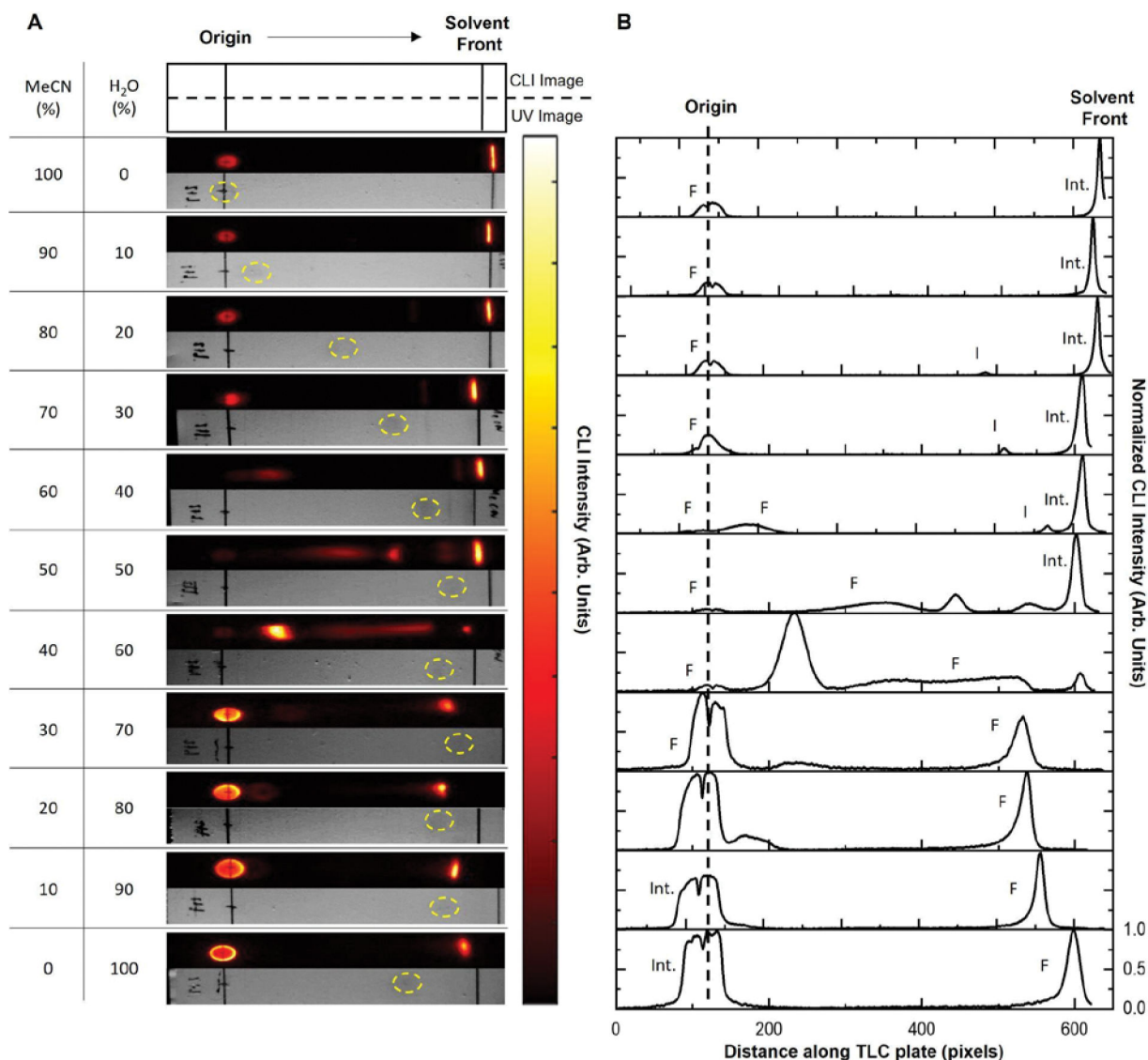
**Figure 5.**
Impact of water composition in aqueous mobile phases (MeCN:H$_2$O) on the migration of [$^{18}$F]FET-intermediate and FET. **(A)** Images of TLC plates. For each mobile phase composition, a CLI image of the TLC plate spotted with crude [$^{18}$F]FET-intermediate is shown (top), along with a UV image of an adjacent lane spotted with FET reference standard (bottom). The FET standard band is enclosed with a yellow dashed line for clarity. **(B)** Normalized TLC chromatograms generated from the CLI images. F denotes [$^{18}$F]TBAF, Int denotes [$^{18}$F]FET-intermediate, and I denotes impurity.

**Table 1.**

Mobile phases reported in the literature for silica-based TLC separation of various radiopharmaceuticals.

| Radiopharmaceutical | Aqueous Mobile Phase | Non-Aqueous Mobile Phase |
|---|---|---|
| [18F]Fallypride | (60:40 MeCN: 25 mM NH$_4$HCO$_2$, 1% TEA)[10,11], (95:5 MeCN:H$_2$O)[17], (90:10 MeCN:H$_2$O)[18] | (10:90 MeOH:DCM)[19], (50:50 MeOH:EtOAc, 1% TEA)[20] |
| [18F]FET | (80:20 MeCN:H$_2$O)[10,21], (67:16.5:16.5 MeCN:MeOH:H$_2$O)[22] | (90:10 MeOH:AcOH)[23], (67:33 Hexanes:EtOAc)[24] |
| [18F]FBB | (90:10 MeCN:H$_2$O)[25] | NR |
| [18F]FDOPA | (95:5 MeCN:H$_2$O)[26], (67:16.5:16.5 MeCN:MeOH:H$_2$O)[27] | (90:10 DCM:EtOAc)[28], (40:60 EtOAc:Et$_2$O)[29] |
| [18F]FEPPA | NR | (8:10:82 MeOH:Hexanes:EtOAc)[30] |
| [18F]FPEB | NR | (95:5 EtOAc:EtOH)[31] |
| [18F]FLT | (95:5 MeCN:H$_2$O)[17,32] | (90:10 DCM:MeOH)[33] |
| [18F]FMZ | (80:15:5 EtOAc:EtOH:H$_2$O)[34,35] | (80:20 EtOAc:EtOH)[36] |
| [18F]FMISO | NR | (95:5 MeOH:NH$_4$)[32], (MeOH)[37] |
| [18F]FNB | (60:40 MeCN:H$_2$O)[38] | NR |
| [18F]FBA | (95:5 MeCN:H$_2$O)[38] | (67:33 Hexanes:EtOAc)[39] |
| [18F]DFA | (95:5 MeCN:H$_2$O)[38] | NR |
| [18F]AlF-2-AMPDA-HB | (75:25 MeCN:H$_2$O)[40] | NR |
| [18F]AlF-NOTA-HL | (50:50 MeCN:H$_2$O)[41] | NR |
| [18F]FTP | (20:80 MeOH: 1M NH$_4$OAc)[42] | NR |
| [18F]Altanserin | (80:20 MeCN:H$_2$O)[43] | NR |
| [18F]MPPF | (90:10 MeCN:H$_2$O)[44] | NR |

NR = not reported.

**Table 2.**

Impact of water composition in aqueous mobile phases (MeCN:$H_2O$) on the retention factor ($R_f$) of [$^{18}$F]fluoride.

| MeCN (%) | H$_2$O (%) | R$_f$ |
|---|---|---|
| 100 | 0 | 0.0 |
| 90 | 10 | 0.0 |
| 80 | 20 | 0.0 |
| 70 | 30 | 0.0 |
| 60 | 40 | 0.0, 0.13 |
| 50 | 50 | 0.0, 0.44 |
| 40 | 60 | 0.0, 0.76 |
| 30 | 70 | 0.0, 0.83 |
| 20 | 80 | 0.92 |
| 10 | 90 | 0.92 |
| 0 | 100 | 0.93 |

**Table 3.**

Impact of water composition in aqueous mobile phases (MeCN:$H_2O$) on the Rf of [$^{18}$F]TBAF.

| MeCN (%) | $H_2O$ (%) | $R_f$ |
|---|---|---|
| 100 | 0 | 0.0 |
| 90 | 10 | 0.0 |
| 80 | 20 | 0.0 |
| 70 | 30 | 0.0 |
| 60 | 40 | 0.0, 0.16 |
| 50 | 50 | 0.0, 0.40 |
| 40 | 60 | 0.0, 0.53 |
| 30 | 70 | 0.0, 0.77 |
| 20 | 80 | 0.88 |
| 10 | 90 | 0.92 |
| 0 | 100 | 0.93 |

**Table 4.**

Impact of water composition in aqueous mobile phases (MeCN:H$_2$O) on the R$_f$ of different radiochemical analytes in the crude synthesis of [$^{18}$F]Fallypride. The R$_f$ of [$^{18}$F]Fallypride was confirmed by parallel spotting of [$^{19}$F]Fallypride.

| MeCN (%) | H$_2$O (%) | R$_f$ values | | |
| --- | --- | --- | --- | --- |
| | | [$^{18}$F]TBAF | [$^{18}$F]Fallypride | Impurity |
| 100 | 0 | 0.0 | 0.07 | 0.75 |
| 90 | 10 | 0.0 | 0.27 | 0.84 |
| 80 | 20 | 0.0 | 0.50 | 0.86 |
| 70 | 30 | 0.0 | 0.68 | 0.90 |
| 60 | 40 | 0.0, 0.19 | 0.57 | 0.79 |
| 50 | 50 | 0.0, 0.40 | 0.40 | ND |
| 40 | 60 | 0.0, 0.53 | 0.18 | ND |
| 30 | 70 | 0.0, 0.77 | 0.10 | ND |
| 20 | 80 | 0.88 | 0.05 | ND |
| 10 | 90 | 0.92 | 0.0 | ND |
| 0 | 100 | 0.93 | 0.0 | ND |

ND = Not discernable.

**Table 5.**

Impact of water composition in aqueous mobile phases (MeCN:$H_2O$) on the $R_f$ of different radiochemical analytes in the crude synthesis of [18F]FMZ. The $R_f$ of [18F]FMZ was confirmed by parallel spotting of [19F]FMZ.

| MeCN (%) | $H_2O$ (%) | $R_f$ values | | |
| --- | --- | --- | --- | --- |
| | | [18F]TBAF | [18F]FMZ | Impurity |
| 100 | 0 | 0.0 | 0.84 | 0.89 |
| 90 | 10 | 0.0 | 0.89 | 0.79 |
| 80 | 20 | 0.0 | 0.78 | ND |
| 70 | 30 | 0.0 | 0.82 | ND |
| 60 | 40 | 0.0, 0.18 | 0.88 | ND |
| 50 | 50 | 0.0, 0.42 | 0.88 | ND |
| 40 | 60 | 0.0, 0.58 | 0.82 | ND |
| 30 | 70 | 0.0, 0.80 | 0.70 | ND |
| 20 | 80 | 0.84 | 0.60 | ND |
| 10 | 90 | 0.84 | 0.53 | ND |
| 0 | 100 | 0.93 | 0.18 | ND |

ND = Not discernable

**Table 6.**

Impact of water composition in aqueous mobile phases (MeCN:H$_2$O) on the R$_f$ of different radiochemical analytes in the crude synthesis of [$^{18}$F]FET.

| MeCN (%) | H$_2$O (%) | R$_f$ values | | |
|---|---|---|---|---|
| | | [$^{18}$F]TBAF | [$^{18}$F]FET-intermediate | FET |
| 100 | 0 | 0.0 | 0.97 | 0.0 |
| 90 | 10 | 0.0 | 0.95 | 0.11 |
| 80 | 20 | 0.0 | 0.97 | 0.48 |
| 70 | 30 | 0.0 | 0.95 | 0.69 |
| 60 | 40 | 0.0, 0.13 | 0.95 | 0.79 |
| 50 | 50 | 0.0, 0.43 | 0.91 | 0.80 |
| 40 | 60 | 0.0, 0.55 | ND | 0.82 |
| 30 | 70 | 0.0, 0.77 | ND | 0.82 |
| 20 | 80 | 0.79 | ND | 0.81 |
| 10 | 90 | 0.82 | 0.0 | 0.76 |
| 0 | 100 | 0.90 | 0.0 | 0.71 |

ND = Not discernable.